第 54 卷第 4 期
2026 年 4 月

硅 酸 盐 学 报
JOURNAL OF THE CHINESE CERAMIC SOCIETY

Vol. 54，No. 4
April，2026

http://jccsoc.cbpt.cnki.net

DOI：10.14062/j.issn.0454-5648.20250560

Eu 掺杂 $MgO–P_2O_5–B_2O_3$ 玻璃的光学、发光和闪烁性能

KAI Okazaki, AKIHIRO Nishikawa, DAISUKE Nakauchi, TAKUMI Kato,
NORIAKI Kawaguchi, TAKAYUKI Yanagida

(奈良先端科学技术学院(NAIST)，奈良县生驹市 630-0192，日本)

摘　要：通过熔融淬火法制备了未掺杂和掺杂 Eu 的 $MgO–P_2O_5–B_2O_3$ 玻璃，并研究了它们的光学和闪烁性能。制备的样品具有 70%~90%的透射率。由于在紫外–可见光和 X 射线下 Eu^{2+}发生 $4f^65d^1–4f^7$ 跃迁并产生发光。当在 320 nm 激发、在 350～560 nm 监测时 0.1%、0.3%、1.0%和 2.0% (摩尔分数)Eu 掺杂的 $MgO-P_2O_5-B_2O_3$ 玻璃的光致发光量子产率分别为 46.7%、37.2%、20.4%和 9.3%。在未掺杂、0.1%、0.3%、1.0%和 2.0%掺杂 Eu 的样品中，计算出在 2 ms X 射线照射后 20 ms 的余辉水平分别为 1700×10^{-6}、4500×10^{-6}、3400×10^{-6}、800×10^{-6} 和 160×10^{-6}。使用合成的 $MgO–P_2O_5–B_2O_3$ 玻璃测量 ^{241}Am α 射线脉冲高度谱。根据比较样品和参照物(Gd_2SiO_5、*LY*:8000 光子/MeV)的全吸收峰位置，0.3%、1.0%和 2.0%掺铕样品的光产额(*LY*)计算分别为 70、150 和 40 个光子/5.5 MeV。

关键词：闪烁；光致发光；二价铕离子；辐射检测
中图分类号：TQ175　　**文献标志码**：A　　**文章编号**：0454–5648(2026)04–1299–08
网络出版时间：2025–11–28

1 Introduction

Scintillators are functional materials that immediately emit low-energy photons after absorbing high-energy ionizing radiations such as X-rays, α-particles, and neutrons[1–3]. They are applied in various fields as radiation detectors, for example, medical[4–5], security[6–7], astrophysics[8–9], and well logging[10–11]. The requirement for scintillators varies depending on each application; hence, scintillators with appropriate characteristics are selected and used. In the classification of material forms, crystals[12–13], polymers[14–15], ceramics[16–17], and glasses[18–19] are representative. Glasses have many advantages, such as low manufacturing costs, ease of formability, high optical transparency, and high compositional tunability. A ^{6}Li-glass scintillator doped with Ce is a commercial glass scintillator[20], and it has been used for thermal neutron detections owing to ^{6}Li(n,a)^{3}H neutron capture reactions. In general, the ^{3}He counter is used in practice for neutron detections; however, the depletion of the ^{3}He supply has driven vigorous research and development of alternative materials[21].

^{10}B-contained glasses have an advantage of their larger thermal neutron capture cross section (3840 barn) than ^{6}Li (940 barn) for using in thermal neutron detections, and many basic studies of borate glasses have been conducted for the application[22–24]. In this study, we focused on $MgO–P_2O_5–B_2O_3$ glass systems. They are composed of light elements; hence, neutron detection signals can be easily distinguished from noise due to X- and γ-rays. Furthermore, alkali-earth-embedded $P_2O_5–B_2O_3$ glasses realize high optical transparency with good chemical durability[25–26]. As luminescence centers, Eu was selected. Eu exists in two different states: Eu^{2+} in reduction states and Eu^{3+} in oxidation states. The former shows broad emission bands with fast decay times of ~μs, whereas the latter shows sharp emission bands with slow decay times of ~ms. In general, Eu^{3+} is governed in the glasses prepared in an air atmosphere; however, alkali-earth-embedded $P_2O_5–B_2O_3$ glasses can exhibit Eu^{2+} owing to the localized reducing atmosphere generated by NH_3 derived from the raw material ($NH_4H_2PO_4$)[27]. Here, Eu-doped $MgO–P_2O_5–B_2O_3$ glasses with various concentrations of Eu were synthesized by the conventional melt quenching technique in air, and their optical, photoluminescence (PL), and scintillation properties were examined.

2 Experimental

Undoped and 0.1%, 0.3%, 1.0%, and 2.0% (in mole

收稿日期：2025–07–18。　修订日期：2025–09–16。
基金项目：生物医学工程研究中心合作研究项目，中部电工技术研究基金和岛津科学基金。
第一作者：KAI Okazaki (1998—)，男，博士研究生。

Received date: 2025–07–18.　**Revised date:** 2025–09–16.
First author: KAI Okazaki (1998–), male, Doctoral candidate.
E-mail: okazaki.kai.of0@ms.naist.jp

fraction) Eu-doped $25MgO–30P_2O_5–45B_2O_3$ (MPB) glasses were synthesized by the melt quenching method. Eu_2O_3 (4N, Furuuchi Chemical), $MgCO_3$ (4N, High Purity Chemicals), $NH_4H_2PO_4$ (4N, Sigma-Aldrich), and $(NH_4)_2O·5B_2O_3·8H_2O$ (2N, Kanto Chemical) were mixed with a stoichiometric ratio using an agate mortar, homogeneously. The powders were transferred into an alumina crucible and melted at 1100 ℃ for 1 h with an electrical furnace in air. The melt was flowed onto a preheated stainless-steel plate to quench, and pressed into batches. After that, the glasses were annealed at 400 ℃ for 1 h to remove thermal and mechanical strains. The surfaces of the glasses were polished for the following optical and scintillation measurements. The glass transition temperature (T_g) of the undoped sample was measured with a TG-DTA system (Hitachi High-Tech Corporation, STA7200).

The powder X-ray diffraction (XRD) patterns were measured using a diffractometer (Rigaku, MiniFlex600). Diffuse transmission spectra were measured using a spectrophotometer (Shimadzu, SolidSpec-3700). PL excitation (PLE) and emission spectra, PL quantum yields (*QY*s), and PL decay curves were measured using a Quantaurus-QY (Hamamatsu Photonics, C11347) and Quantaurus-τ (Hamamatsu Photonics, C11367). Scintillation spectra, scintillation decay curves, afterglow curves under X-ray irradiations, and pulse height spectra of ^{241}Am α-rays and ^{137}Cs γ-rays were measured with our original setups[28–29]. The monitored wavelengths in scintillation decay curves and afterglow curves under X-ray irradiations were 190–650 nm with a photomultiplier tube (Hamamatsu Photonics, R7400P-06).

3 Results and discussion

The appearances of undoped and Eu-doped MPB glasses are shown in Fig. 1. The surfaces of the samples were polished, and the sizes were adjusted to 4–5 mm in length and 1 mm in thickness. They looked transparent and included some bubbles. Under ultraviolet (UV) light at 360 nm, Eu-doped samples showed bluish-red light.

Some parts of the glasses were crushed into powder and used for the XRD measurements. The XRD patterns of the samples are shown in Fig. 2. Precipitations of crystalline phases were not observed in the patterns; hence, the prepared samples formed glass phases with no periodical structures. Fig. 3 shows the DTA curve of the undoped sample. T_g of the undoped sample was estimated at 535 ℃.

Fig. 4 shows the diffuse transmission spectra of the prepared glasses. The transmittances of all the glasses were 70%–90% at 400–700 nm. Both the undoped and Eu-doped samples showed absorption peaks at 200–250 nm; hence, this can be due to the hosts. In addition, absorption peaks emerged at 250–400 nm in Eu-doped samples. The absorption bands at 250–280 nm and 280–400 nm originated from the $4f^7–4f^65d^1$ (T_{2g} and E_g) transitions of Eu^{2+}, respectively[30–31]. An absorption peak due to the $^7F_1–^5D_3$ transitions of Eu^{3+} was confirmed at 415 nm in the spectra of 2% Eu[32].

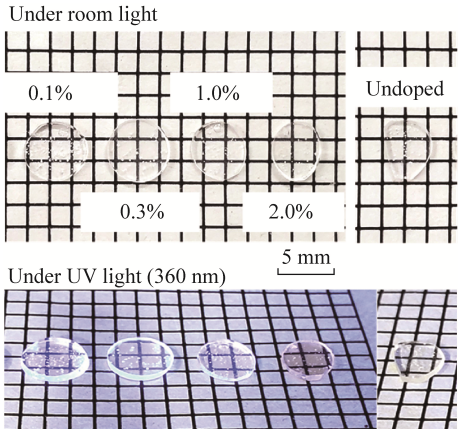

Fig. 1 Photographs of 0.1%, 0.3%, 1.0%, and 2.0% (in mole fraction) Eu-doped and undoped MPB glasses under room light and UV light (360 nm)

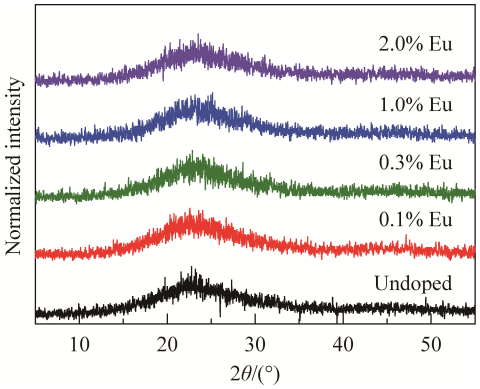

Fig. 2 XRD patterns of undoped and Eu-doped MPB glasses

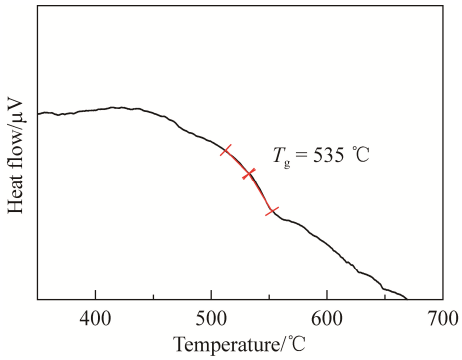

Fig. 3 DTA curve of undoped MPB glass

Fig. 5 shows the PLE and PL spectra of undoped and Eu-doped MPB glasses. The undoped sample showed a broad emission peak at 300–550 nm under excitation at 250–290 nm. Some B_2O_3-based glasses showed broad emissions with PLE peaks at 250–290 nm[33], and the PLE spectral features were similar to the spectra in this study. Therefore, the emission was considered to be derived from the recombination of electrons with O^- hole centers. In contrast, broad emission bands due to the

electronic transitions of Eu^{2+} were observed at 400–600 nm under excitation bands at 250–410 nm in the Eu-doped samples[27]. The emission peaks were slightly shifted to the low-energy side as the Eu-concentration increased. Generally, emissions due to Eu^{2+} were difficult to be observed in the glasses prepared in air because of the oxidizing atmosphere. The emissions appeared owing to the localized reduction atmosphere, which derived from $NH_4H_2PO_4$ and $(NH_4)_2O·5B_2O_3·8H_2O$. Additionally, sharp emission bands due to the electronic transitions of Eu^{3+} were observed at 550–700 nm under several excitations at 380–410 nm[34]. The PL *QY*s were measured and shown in Table 1. When monitored at 350–560 nm, PL *QY*s decreased as the Eu-concentration increased, whereas the values showed no significant changes against Eu-concentrations when monitored at 580–750 nm. The tendency of the decrease in PL *QY*s is considered to be derived from concentration quenching due to cross-relaxations of Eu^{2+}.

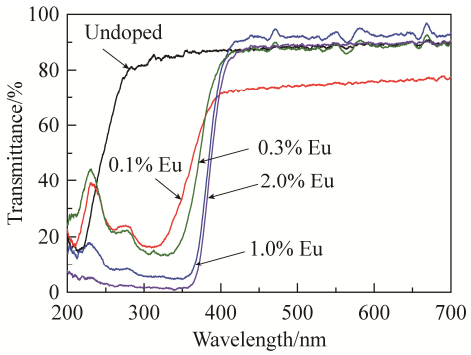

Fig. 4　Diffuse transmission spectra of undoped and Eu-doped MPB glasses

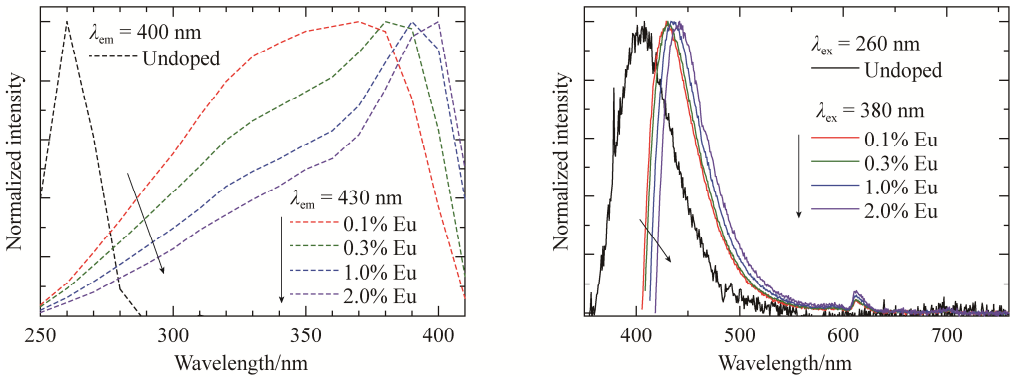

Fig. 5　PLE (left) and PL (right) spectra of undoped and Eu-doped MPB glasses

Table 1　PL *QY*s of undoped and Eu-doped MPB glasses

Sample	PL *QY*s/%		
	Ex. 260 nm Em. 350–600 nm	Ex. 320 nm Em. 350–560 nm	Ex. 390 nm Em. 580–750 nm
Undoped	1.7		
0.1% Eu		46.7	1.3
0.3% Eu		37.2	1.5
1.0% Eu		20.4	1.2
2.0% Eu		9.3	0.8

Fig. 6 shows the PL decay curves of Eu-doped MPB glasses. When excitation and monitored wavelengths were respectively set to 340 nm and 420 nm, the obtained decay curves were fitted by a sum of two exponential functions. The PL decay time constants of both the fast (0.2–0.5 μs) and slow (0.7–1.2 μs) components were similar to those of other Eu-doped phosphors; hence, they were reasonable as $4f^65d^1(T_{2g})–4f^7$ and $4f^65d^1(E_g)–4f^7$ transitions of Eu^{2+}[35–37]. The decay time constants became faster as the Eu concentration increased. Based on the result and the tendency of PL *QY*s (Tab. 1), it can be due to the concentration quenching of Eu^{2+}. PL decay curves, with decay time constants of 1–3 ms, were measured by monitoring 620 nm under excitation at 365–390 nm. The decay curves were approximated by a sum of three exponential functions. The fastest components were derived from the instrumental response function (IRF). The PL decay time constants were almost the same values as those of Eu-doped glasses, which were reported in past studies[38–39]; therefore, they were attributed to the $^5D_0–^7F_2$ transitions of Eu^{3+}.

Fig. 7 shows the X-ray-induced scintillation spectra of undoped and Eu-doped MPB glasses. Undoped samples showed the broad emission peak at 250–500 nm, although the signal-to-noise ratio was low. Similar broad emission peaks were confirmed in the PL spectra; therefore, the emission can be related to the recombination of electrons with O^- hole centers. Eu-doped samples showed emission peaks at 350–500 nm. These emission wavelengths were consistent with those of the PL spectra. Furthermore, the spectral features were almost the same as those of Eu-doped scintillators. Thus, the emission origin can be the $4f^65d^1–4f^7$ transitions of Eu^{2+} [34, 40]. In addition, sharp emission peaks appeared at 570–650 nm. They are derived from the $^5D_0–^7F_{0,1}$ (580 nm), $^5D_0–^7F_2$ (620 nm), $^5D_0–^7F_3$ (650 nm) transitions of Eu^{3+}[41–42]. The relative intensities of the emissions due to Eu^{3+} became high as the Eu-concentrations increased. It was due to the concentration quenching of the emissions of Eu^{2+}.

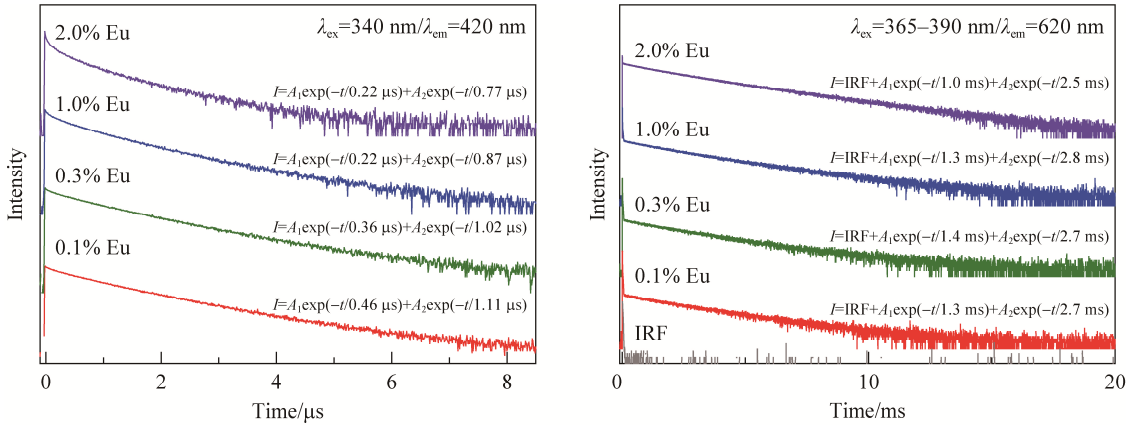

Fig. 6 PL decay curves of Eu-doped MPB glasses monitored at 420 nm under excitation at 340 nm (left) and monitored at 620 nm under excitation at 365–390 nm (right)

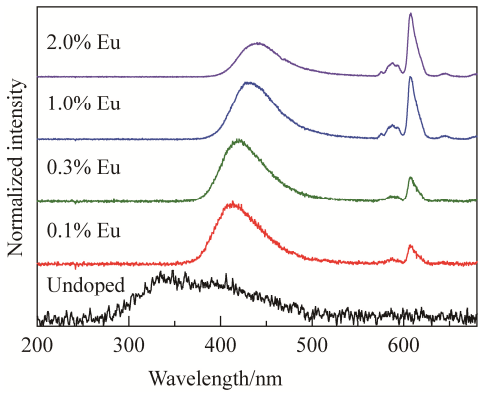

Fig. 7 X-ray-induced scintillation spectra of undoped and Eu-doped MPB glasses

Fig. 8 shows the X-ray-induced scintillation decay curves of the Eu-doped MPB glasses. The scintillation decay curves in the left figure were measured with the time range of the μs order. The decay curves were fitted by a sum of two exponential functions. The fast components were induced by the IRF. The slow components had the scintillation decay time constants of 0.1–0.6 μs. Whereas the decay time constants of 0.1% Eu-doped samples were faster than previous reports on scintillation of Eu^{2+}-doped glasses, these values were reasonable as the $4f^65d^1$–$4f^7$ transitions of Eu^{2+}. Furthermore, the values were similar to those confirmed in PL decay measurements (Fig. 6). The scintillation decay curves in the right figure were measured with a time range of the ms order. The obtained decay curves were composed of a sum of two exponential functions. Both the fast and slow components were derived from the 4f–4f transitions of Eu^{3+}.

Fig. 9 shows the afterglow curves after X-ray irradiation of 2 ms of the prepared samples. Afterglow levels (*AL*s) were calculated to estimate the amounts of trapped carriers that were re-excited by thermal stimulations at room temperature. The calculation formula is as follows: $AL = (I_{20}–I_{BG})/(I_{MAX}–I_{BG})$, where I_{20}, I_{BG}, and I_{MAX} are respectively intensities at 20 ms passed after X-ray irradiations, background signals before X-ray irradiations, and intensities during X-ray irradiations. The obtained *AL*s of undoped and 0.1%, 0.3%, 1.0%, and 2.0% Eu-doped glasses were respectively 1700×10^{-6}, 4500×10^{-6}, 3400×10^{-6}, 800×10^{-6}, and 160×10^{-6}. The *AL*s increased by Eu-doping, whereas they decreased as Eu-concentrations became high. It can indicate that the number of trapping centers at shallow levels decreased owing to the high concentration of Eu-doping. The *AL*s of the 1% and 2% Eu-doped glasses were comparable to the value of Tl-doped CsI (~300×10^{-6})[43], which is one of the commercial scintillators for X-ray detection.

Fig. 10 shows the pulse height spectra of ^{241}Am α-rays (5.5 MeV) measured by using the prepared MPB glasses and that of ^{137}Cs γ-rays measured by using Ce-doped Gd_2SiO_5 (GSO, 8000 photons/MeV) as a reference. The glasses did not show clear energy peaks due to thermal neutrons; hence, spectra of ^{241}Am γ-rays were measured to investigate the light yields (*LY*) of the glasses. Here, the energy peak due to ^{241}Am γ-rays did not appear. The 0.3%, 1.0%, and 2.0% Eu-doped glasses showed clear full energy absorption peaks. *LY*s of prepared samples were estimated by comparing the channels of full energy absorption peaks with those of a reference. *LY*s of 0.3%, 1.0%, and 2.0% Eu-doped MPB glasses were respectively calculated to be 70, 150, and 40 photons/5.5 MeV-α. Scintillation is understood to be composed of three processes: creation of a large number of electrons and holes through absorptions of ionizing radiations, energy transportation of the numerous secondary electrons and holes, and emission at the luminescence centers. Based on the Robins' model[44], the *LY* can be explained by the following equation: $LY \propto (1/\beta E_g) \times S \times QY$. Here, β, E_g, and S are respectively the numerical coefficient, bandgap energy, and energy transport efficiency. The 1% Eu-doped sample showed the highest *LY* in the prepared samples, although its *QY* was lower than those of the 0.1% and 0.3% Eu-doped samples, as shown in Table 1. From the obtained results of *LY*s and *QY*s, it can be suggested that the *S* of the 1%

(in mole) Eu-doped sample was higher than that of the 0.1% and 0.3% Eu-doped samples. Empirically, the *AL*, which was proportional to the number of trapped secondary electrons and holes, of the 1% (in mole) Eu-doped sample was superior to that of the 0.1% and 0.3% Eu-doped samples. When the *LY*s of prepared samples were compared with those of a commercial glass scintillator for thermal neutron detections (GS20, 6000 photons/n), they were significantly lower as the *QY*s of prepared samples were approximately half of the GS20 (90%)[45]. To improve the *QY*s and *LY*s, it can be one of the strategies that the synthesis environment changes to a reduction environment from the air.

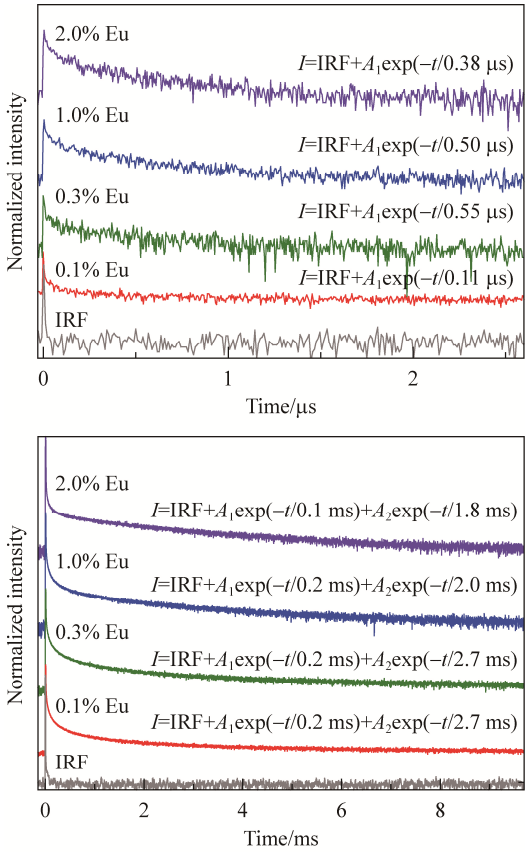

Fig. 8　X-ray-induced scintillation decay curves of Eu-doped MPB glasses

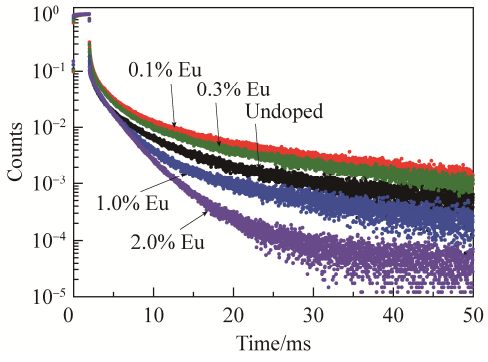

Fig. 9　Afterglow curves of undoped and Eu-doped MPB glasses after X-ray irradiation of 2 ms

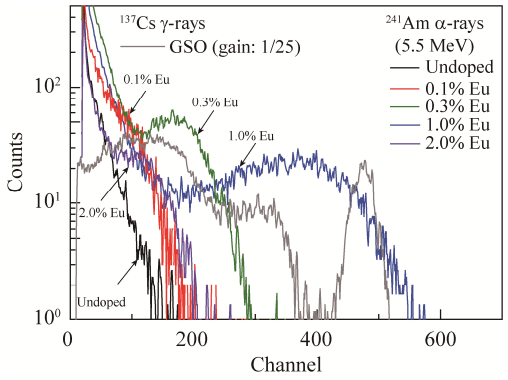

Fig. 10　Pulse height spectra of ^{241}Am α-rays measured using undoped and Eu-doped MPB glasses and ^{137}Cs γ-rays measured using GSO as a reference

Table 2　*LY*s of undoped and Eu-doped MPB glasses

Sample	*LY*s/(photons·5.5 MeV^{-1})
Undoped	
0.1% Eu	
0.3% Eu	70
1.0% Eu	150
2.0% Eu	40

4　Conclusions

Undoped and Eu-doped MPB glasses were synthesized by the conventional melt quenching method. All the samples showed halo peaks with no periodic patterns in XRD measurements. The transmittances of all glasses were 70%–90%, and absorptions due to electronic transitions of Eu^{2+} and Eu^{3+} were observed. All the samples showed luminescence, which originated from the $4f^65d^1–4f^7$ transitions of Eu^{2+}. In addition, the obtained PL and scintillation decay time constants were reasonable values as the $4f^65d^1–4f^7$ transitions of Eu^{2+}. PL *QY*s of 0.1%, 0.3%, 1.0%, and 2.0% Eu-doped samples were respectively calculated to be 46.7%, 37.2%, 20.4%, and 9.3% when monitored at 350–560 nm under excitation at 320 nm. *AL*s at 20 ms passed after X-ray irradiations of 2 ms were obtained to be 1700×10^{-6}, 4500×10^{-6}, 3400×10^{-6}, 800×10^{-6}, and 160×10^{-6} in undoped, 0.1%, 0.3%, 1.0%, and 2.0% Eu-doped samples, respectively. Pulse height spectra of ^{241}Am α-rays were measured using the prepared samples. *LY*s of 0.3%, 1.0%, and 2.0% Eu-doped samples were respectively determined to be 70, 150 photons/5.5 MeV, and 40 photons/5.5 MeV. Although thermal neutrons cannot be measured by using the prepared Eu-doped MPB glasses, the compositions of MPB glasses have the potential to be candidates for scintillators for thermal neutron detection applications because thermal neutrons were observed through α-ray detections in the case of the neutron capture reactions of ^{10}B.

References:

[1] VAN EIJK C W E. Development of inorganic scintillators[J]. Nucl Instrum Meth Phys Res Sect A Accel Spectrometers Detect Assoc

Equip, 1997, 392(1–3): 285–290.

[2] WEBER M J. Inorganic scintillators: Today and tomorrow[J]. J Lumin, 2002, 100(1–4): 35–45.

[3] DERENZO S E, WEBER M J, BOURRET-COURCHESNE E, et al. The quest for the ideal inorganic scintillator[J]. Nucl Instrum Meth Phys Res Sect A Accel Spectrometers Detect Assoc Equip, 2003, 505(1–2): 111–117.

[4] VAN EIJK C W E. Inorganic scintillators in medical imaging detectors[J]. Nucl Instrum Meth Phys Res Sect A Accel Spectrometers Detect Assoc Equip, 2003, 509(1–3): 17–25.

[5] KHOSHAKHLAGH M, ISLAMIAN J P, ABEDI S M, et al. Development of scintillators in nuclear medicine[J]. World J Nucl Med, 2015, 14(3): 156–159.

[6] RYZHIKOV V D, OPOLONIN A D, PASHKO P V, et al. Instruments and detectors on the base of scintillator crystals ZnSe(Te), CWO, CsI(Tl) for systems of security and customs inspection systems[J]. Nucl Instrum Meth Phys Res Sect A Accel Spectrometers Detect Assoc Equip, 2005, 537(1–2): 424–430.

[7] AN B Y, DENG Y J, JIN Z W, et al. Scintillators for neutron detection and imaging: Advances and prospects[J]. Adv Funct Mater, 2025, 35(19): 2422522.

[8] LAWRENCE D J, BARBIER L M, BEATTY J J, et al. Large-area scintillating-fiber time-of-flight/hodoscope detectors for particle astrophysics experiments[J]. Nucl Instrum Meth Phys Res Sect A Accel Spectrometers Detect Assoc Equip, 1999, 420(3): 402–415.

[9] BLOSER P F, LEGERE J S, BANCROFT C M, et al. Testing and simulation of silicon photomultiplier readouts for scintillators in high-energy astronomy and solar physics[J]. Nucl Instrum Meth Phys Res Sect A Accel Spectrometers Detect Assoc Equip, 2014, 763: 26–35.

[10] MELCHER C L. Scintillators for well logging applications[J]. Nucl Instrum Meth Phys Res Sect B Beam Interact Mater At, 1989, 40–41: 1214–1218.

[11] MELCHER C L, SCHWEITZER J S, MANENTE R S, et al. Applicability of GSO scintillators for well logging[J]. IEEE Trans Nucl Sci, 1991, 38(2): 506–509.

[12] WEBER M J. Scintillation: Mechanisms and new crystals[J]. Nucl Instrum Meth Phys Res Sect A Accel Spectrometers Detect Assoc Equip, 2004, 527(1–2): 9–14.

[13] YANAGIDA T, KATO T, NAKAUCHI D, et al. Fundamental aspects, recent progress and future prospects of inorganic scintillators[J]. Jpn J Appl Phys, 2023, 62(1): 010508.

[14] SALIMGAREEVA V N, KOLESOV S V. Plastic scintillators based on polymethyl methacrylate: A review[J]. Instrum Exp Tech, 2005, 48(3): 273–282.

[15] KOSHIMIZU M. Composite scintillators based on polymers and inorganic nanoparticles[J]. Funct Mater Lett, 2020, 13(6): 2030003.

[16] GRESKOVICH C, DUCLOS S. Ceramic scintillators[J]. Annu Rev Mater Sci, 1997, 27: 69–88.

[17] YANAGIDA T, TAKAHASHI H, ITO T, et al. Evaluation of properties of YAG (Ce) ceramic scintillators[J]. IEEE Trans Nucl Sci, 2005, 52(5): 1836–1841.

[18] BOLLINGER L M, THOMAS G E, GINTHER R J. Neutron detection with glass scintillators[J]. Nucl Instrum Meth, 1962, 17(1): 97–116.

[19] XU W X, ZHENG Y, LIU X F, et al. Manipulation of coupled X-ray-excited persistent luminescence and upconversion in Er^{3+} doped fluoride nanoparticles for multifaceted applications[J]. Laser Photonics Rev, 2024, 18(8): 2400147.

[20] FAVALLI A, WIGGINS B W, ILIEV M, et al. Next-generation neutron detection using a 6Li glass scintillator composite[J]. Commun Phys, 2025, 8: 10.

[21] KOUZES R T, LINTEREUR A T, SICILIANO E R. Progress in alternative neutron detection to address the helium-3 shortage[J]. Nucl Instrum Meth Phys Res Sect A Accel Spectrometers Detect Assoc Equip, 2015, 784: 172–175.

[22] BISHAY A M. Glass scintillator for neutron detection[J]. J Am Ceram Soc, 1961, 44(5): 231–233.

[23] APPLEBY G A, VONTOBEL P. Optimisation of lithium borate–barium chloride glass-ceramic thermal neutron imaging plates[J]. Nucl Instrum Meth Phys Res Sect A Accel Spectrometers Detect Assoc Equip, 2008, 594(2): 253–256.

[24] SAHA S, KIM H J, ARYAL P, et al. Synthesis and characterization of borate glasses for thermal neutron scintillation and imaging[J]. Radiat Meas, 2020, 134: 106319.

[25] MARTIN V, OKADA G, TONCHEV D, et al. Samarium-doped oxyfluoride borophosphate glasses for X-ray dosimetry in Microbeam Radiation Therapy[J]. J Non Cryst Solids, 2013, 377: 137–141.

[26] GUIMARÃES NETO F, DA SILVA PALÁCIOS R, SATO F, et al. Investigation of the influence of SrO addition on the bioactivity of $CaONa_2O$-P_2O_5-B_2O_3 glass system[J]. Materialia, 2022, 26: 101582.

[27] QIU K, XU S C, TIAN H, et al. Composition-induced valence variation of europium and the photoluminescence properties for Eu^{2+} doped borophosphate luminous glass in air[J]. Optoelectron Lett, 2011, 7(5): 350–353.

[28] YANAGIDA T, KAMADA K, FUJIMOTO Y, et al. Comparative study of ceramic and single crystal Ce: GAGG scintillator[J]. Opt Mater, 2013, 35(12): 2480–2485.

[29] YANAGIDA T, FUJIMOTO Y, ITO T, et al. Development of X-ray-induced afterglow characterization system[J]. Appl Phys Express, 2014, 7(6): 062401.

[30] NOGAMI M, YAMAZAKI T, ABE Y. Fluorescence properties of Eu^{3+} and Eu^{2+} in Al_2O_3–SiO_2 glass[J]. J Lumin, 1998, 78(1): 63–68.

[31] MISBAH M H, GHONIEM M G, AL-FARRAJ E S, et al. Mixed former effect in barium borophosphate glasses on the red (Eu^{3+})-blue (Eu^{2+}) emission for LEDs[J]. Ceram Int, 2024, 50(22): 47805–47812.

[32] NAKAMORI R, KAWANO N, TAKAKU A, et al. Preparation and scintillation properties of the Eu^{3+}-activated SrO–Al_2O_3–TeO_2 glasses[J]. Mater Res Bull, 2022, 145: 111547.

[33] KINDRAT I I, PADLYAK B V, DRZEWIECKI A. Intrinsic luminescence of un-doped borate glasses[J]. J Lumin, 2017, 187: 546–554.

[34] HUANG Y L, JANG K, WANG X G, et al. Optical properties of Eu^{2+}-doped strontium borate glasses containing F^- and Li^+ ions[J]. J Rare Earths, 2008, 26(4): 490–494.

[35] SUN X Y, LE X C, XIAO Z H, et al. Self-reduction of Eu^{3+} to Eu^{2+} in europium-doped $Li_2B_4O_7$ glass prepared in air[J]. J Am Ceram Soc, 2020, 103(5): 3119–3125.

[36] HERRMANN A, SIMON A, RÜSSEL C. Preparation and luminescence properties of Eu^{2+}-doped $BaSi_2O_5$ glass-ceramics[J]. J Lumin, 2012, 132(1): 215–219.

[37] YUAN B L, HUANG Y L, YU Y M, et al. Luminescence and structure of Eu^{2+}-doped $Ba_2CaMg_2Si_6O_{17}$[J]. Ceram Int, 2012, 38(3): 2219–2223.

[38] RAJARAMAKRISHNA R, CHAIPHAKSA W, GARIMA, et al. X-ray luminescence, photoluminescence, and radiation shielding properties

of europium-doped oxide glasses for red light-emitting device applications[J]. Phys Status Solidi A, 2023, 220(10): 2200411.

[39] ARUNKUMAR S, VENKATA KRISHNAIAH K, MARIMUTHU K. Structural and luminescence behavior of lead fluoroborate glasses containing Eu^{3+} ions[J]. Phys B Condens Matter, 2013, 416: 88–100.

[40] FU J, KOBAYASHI M, SUGIMOTO S, et al. Scintillation from Eu^{2+} in nanocrystallized glass[J]. J Am Ceram Soc, 2009, 92(9): 2119–2121.

[41] LUEWARASIRIKUL N, SARACHAI S, KOTHAN S, et al. Eu^{3+}-doped gadolinium borate glass system development for optical and scintillation applications[J]. Optik, 2023, 292: 171385.

[42] KHRONGCHAIYAPHUM F, WANTANA N, KANSIRIN S, et al. Eu^{3+} doped Na_2O-Gd_2O_3-BaO-B_2O_3-P_2O_5 glasses for X-ray scintillator application[J]. Optik, 2023, 292: 171355.

[43] NAKAUCHI D, KATO T, KAWAGUCHI N, et al. Characterization of Eu-doped Ba_2SiO_4, a high light yield scintillator[J]. Appl Phys Express, 2020, 13(12): 122001.

[44] ROBBINS D J. On predicting the maximum efficiency of phosphor systems excited by ionizing radiation[J]. J Electrochem Soc, 1980, 127(12): 2694–2702.

[45] YANAGIDA T, UEDA J, MASAI H, et al. Optical and scintillation properties of Ce-doped $34Li_2O–5MgO–10Al_2O_3–51SiO_2$ glass[J]. J Non Cryst Solids, 2016, 431: 140–144.

作者贡献声明：

KAI Okazaki：提出研究方向，设计论文框架并撰写稿件；

AKIHIRO Nishikawa：参与数据整理与分析，完善论文框架并修改稿件；

DAISUKE Nakauchi：参与数据分析，完善论文框架并修改稿件；

TAKUMI Kato：参与数据分析，完善论文框架并修改稿件；

NORIAKI Kawaguchi：完善论文框架并修改稿件；

TAKAYUKI Yanagida：指导研究工作与研究方向，完善论文框架并修改稿件。

Optical, Luminescence, and Scintillation Properties of Eu-Doped $MgO–P_2O_5–B_2O_3$ Glasses

KAI Okazaki, *AKIHIRO Nishikawa*, *DAISUKE Nakauchi*, *TAKUMI Kato*, *NORIAKI Kawaguchi*, *TAKAYUKI Yanagida*
(Nara Institute of Science and Technology (NAIST), 8916-5 Takayama-Cho, Ikoma City, Nara 630-0192, Japan)

Extended Abstract

Introduction Scintillators are functional materials that immediately emit low-energy photons after absorbing high-energy ionizing radiations. Glasses have advantages as a material form for scintillator use, such as low manufacturing costs, ease of formability, high optical transparency, and high compositional tunability. A ^{6}Li-glass scintillator doped with Ce is a commercial glass scintillator, and it has been used for thermal neutron detections owing to $^6Li(n,\alpha)^3H$ neutron capture reactions. In general, the ^{3}He counter is used in practice for neutron detections; however, the depletion of the ^{3}He supply has driven vigorous research and development of alternative materials. ^{10}B-contained glasses have an advantage of their large thermal neutron capture cross section (3840 barn). In this study, we focused on $MgO–P_2O_5–B_2O_3$ glass systems. They are composed of light elements; hence, neutron detection signals can be easily distinguished from noise due to X- and γ-rays. Furthermore, alkali-earth-embedded $P_2O_5–B_2O_3$ glasses realize high optical transparency with good chemical durability. As luminescence centers, Eu was selected. Eu exists in two different states: Eu^{2+} in reduction states and Eu^{3+} in oxidation states. The former shows broad emission bands with fast decay times of ~μs, whereas the latter shows sharp emission bands with slow decay times of ~ms. In general, Eu^{3+} is governed in the glasses prepared in an air atmosphere; however, alkali-earth-embedded $P_2O_5–B_2O_3$ glasses can exhibit Eu^{2+} owing to the localized reducing atmosphere generated by NH_3 derived from the raw material ($NH_4H_2PO_4$). Here, Eu-doped $MgO–P_2O_5–B_2O_3$ glasses with various concentrations of Eu were synthesized by the conventional melt quenching technique in air, and their optical, photoluminescence (PL), and scintillation properties were examined.

Methods Undoped and 0.1%, 0.3%, 1.0%, and 2.0% (in mole fraction) Eu-doped $25MgO–30P_2O_5–45B_2O_3$ (MPB) glasses were synthesized by the melt quenching method. Raw materials were homogeneously mixed and transferred into an alumina crucible. The powders were melted at 1100 ℃ for 1 h with an electrical furnace in air. The melt was flowed onto a preheated stainless-steel plate to quench, and pressed into batches. After that, the glasses were annealed at 400 ℃ for 1 h to remove thermal and mechanical strains. The surfaces of the glasses were polished for the following optical and scintillation measurements. The glass transition temperature (T_g) of the undoped sample was measured with a TG-DTA system. The powder X-ray diffraction (XRD) patterns were measured using a diffractometer. Diffuse transmission spectra were measured using a spectrophotometer (Shimadzu, SolidSpec-3700). PL excitation and emission spectra, PL quantum yields (QYs), and PL decay curves were measured using a Quantaurus-QY and Quantaurus-τ. Scintillation spectra, scintillation decay curves, and afterglow curves under X-ray irradiations, and pulse height spectra of ^{241}Am α-rays and ^{137}Cs γ-rays were measured with our original setups.

Results and discussion The appearances of undoped and Eu-doped MPB glasses were transparent and included some bubbles. Under ultraviolet light at 360 nm, Eu-doped samples showed bluish-red light. Some parts of the glasses were crushed into powder and used for the XRD measurements. Precipitations of crystalline phases were not observed in the XRD patterns; hence, the prepared samples formed glass phases with no periodical structures. T_g of the undoped glass was estimated to be 535 ℃. The transmittances of

all the glasses were 70%–90% at 400–700 nm. Both the undoped and Eu-doped samples showed absorption peaks at 200–250 nm; hence, this can be due to the hosts. In addition, absorption peaks emerged at 250–400 nm in Eu-doped samples. The absorption bands at 250–280 nm and 280–400 nm originated from the $4f^7$–$4f^65d^1$ (T_{2g} and E_g) transitions of Eu^{2+}, respectively. An absorption peak due to the $^7F_1$–$^5D_3$ transitions of Eu^{3+} was confirmed at 415 nm in the spectra of 2% Eu. A broad emission band due to the electronic transitions of Eu^{2+} was observed at 400–600 nm under excitation bands at 250–410 nm in the Eu-doped samples. Generally, emissions due to Eu^{2+} are difficult to observe in the glasses prepared in air because of the oxidizing atmosphere. The emissions appeared owing to the localized reduction atmosphere, which derived from $NH_4H_2PO_4$ and $(NH_4)_2O{\cdot}5B_2O_3{\cdot}8H_2O$. When excitation and monitored wavelengths were respectively set to 340 nm and 420 nm, the PL decay curves were fitted by a sum of two exponential functions. The PL decay time constants of both the fast (0.2–0.5 μs) and slow (0.7–1.2 μs) components were similar to those of other Eu-doped phosphors; hence, they are reasonable as $4f^65d^1(T_{2g})$–$4f^7$ and $4f^65d^1(E_g)$–$4f^7$ transitions of Eu^{2+}. Eu-doped samples showed emission peaks at 350–500 nm under X-ray irradiations. These emission wavelengths were consistent with those of the PL spectra. Afterglow levels (*AL*) of undoped and 0.1%, 0.3%, 1.0%, and 2.0% Eu-doped glasses at 20 ms passed after X-ray irradiation of 2 ms were respectively estimated to be 1700×10^{-6}, 4500×10^{-6}, 3400×10^{-6}, 800×10^{-6}, and 160×10^{-6}. Pulse height spectra of ^{241}Am α-rays (5.5 MeV) were measured using the prepared MPB glasses. Eu-doped glasses showed clear full energy absorption peaks. Light yields (*LY*) of 0.3%, 1.0%, and 2.0% Eu-doped MPB glasses were respectively calculated to be 70, 150 photons/5.5 MeV, and 40 photons/5.5 MeV.

Conclusion Eu-doped MPB glasses were synthesized by the conventional melt quenching method. All the samples showed halo peaks with no periodic patterns in XRD measurements. The transmittances were 70%–90%, and absorptions due to electronic transitions of Eu^{2+} and Eu^{3+} were observed. All the samples showed luminescence, which originated from the $4f^65d^1$–$4f^7$ transitions of Eu^{2+}. PL *QY*s of 0.1%, 0.3%, 1.0%, and 2.0% Eu-doped samples were respectively calculated to be 46.7%, 37.2%, 20.4%, and 9.3% when monitored at 350–560 nm under excitation at 320 nm. *AL*s at 20 ms passed after X-ray irradiations of 2 ms were obtained to be 1700×10^{-6}, 4500×10^{-6}, 3400×10^{-6}, 800×10^{-6}, and 160×10^{-6} in undoped, 0.1%, 0. 3%, 1.0%, and 2.0% Eu-doped samples, respectively. Pulse height spectra of ^{241}Am α-rays were measured using the prepared samples. *LY*s of 0.3%, 1.0%, and 2.0% Eu-doped samples were respectively determined to be 70, 150 photons/5.5 MeV, and 40 photons/5.5 MeV.

Keywords scintillation; photoluminescence; divalent europium ion; radiation detection